Available online at www.sciencedirect.com
SCIENCE DIRECT®
Journal of Sound and Vibration 280 (2005) 815–835
JOURNAL OF SOUND AND VIBRATION
www.elsevier.com/locate/jsvi

The dynamics of a slider-crank mechanism with an initially curved coupler under two-component parametric resonance

Yi-Ming Wang

Department of Mechanical Engineering, College of Engineering, National Chunghua Normal University, Chunghua 500, Taiwan

Received 16 June 2003; accepted 17 December 2003

Abstract

The objective of this paper is to study the dynamics and dynamic instability of a slider-crank mechanism with an initially curved coupler under parametric resonance. An attention is given to the phenomena arising due to initial curvature, geometric imperfection, of a connecting rod and modal interactions produced by the existence of two-component parametric resonance.

The two-component parametric resonance can occur, for example, when the fundamental frequency of the flexible part of a slider-crank mechanism is close to one-half of the excitation frequency and simultaneously the difference between the first and the second natural frequencies is near the frequency of excitation.

It is known that for the case of one-component parametric resonance, an initially curved connecting rod enlarges the amplitude of fundamental mode of vibration significantly only if the motion is in the vicinity of the secondary region of instability. In other words, the initial curvature of a coupler plays no effects to the fundamental response of the system if the oscillation is near the primary region of instability. However, result of present study shows that under the condition of two-component parametric resonance, unlike the case of one-component parametric resonance, an initially curved linkage can result significant effects to the vibration of the system even if the motion is close to the primary region of instability. In addition, the result also indicates that the growth of small amplitude vibration into large motion regime occurs if vibrations arise near the boundary of stable region.

1. Introduction

Vibrations of planar mechanisms such as slider-crank mechanisms have been the subjects of many studies. Typically due to the effect of inertia, these elastic links are subject to axial and transverse periodic forces. The mathematical model of the problem then reduces to a multi-degree-of-freedom dynamical system with time-periodic coefficients.

E-mail address: wangym@cc.ncue.edu.tw (Y.-M. Wang).

0022-460X/$ - see front matter © 2004 Elsevier Ltd. All rights reserved.
doi:10.1016/j.jsv.2003.12.037

Badlani and Midha [1] discussed the dynamic instability of a slider-crank mechanism with an initially curved connecting rod under the assumptions of Euler–Bernoulli beam theory. They developed a simple model that neglects the higher modes of vibrations and the interactions among amplitudes. Their results show that the transient and steady state responses of fundamental mode of vibration are amplified significantly by the initial curvature of a coupler only if the steady state response is close to the secondary region of instability.

Zhu and Chen [2] considered the problem of dynamic stability of a slider-crank mechanism with an elastic connecting rod. The authors applied perturbation method to the resulting equations of motion and obtained the Mathieu-type equations. Regions of dynamic instability then are determined on the basis of Mathieu equations.

Hsieh and Shaw [3] analyzed the dynamic response and correspondingly the stability of a slider-crank mechanism by the method of multiple time scales. They discussed the phenomena produced by the occurrence of primary, superharmonic and subharmonic resonances. However, only single resonant mode was considered in their modelling.

Halbig and Beale [4] carried out an experimental model to study the dynamics of slider-crank mechanism at very high speed. They observed the occurrence of parametric resonance and the amplification of response. Fung [5] investigated dynamic responses of a slider-crank mechanism with time-dependent boundary condition.

In Refs. [6,7], the authors studied the dynamic buckling of an imperfect column under different loading conditions. The results of their studies show that, as expected, the initial imperfection amplifies the amplitude of response.

Wang [8] employed the Newtonian method to study the mechanics of a slider-crank mechanism with a perfect straight elastic coupler. The multiple time scales method was applied to study the dynamic instability of response and the occurrence of two-component parametric resonance.

It is known that on the problem of parametric excitations of flexible members for planar mechanisms, the determination of dynamic instability is a crucial question. In general, under the condition of one-component parametric resonance (single mode of parametric resonance), the initial curvature of a coupler to the vibration of a slider-crank mechanism plays an important role only if the vibration is close to the secondary region of instability. In other words, the effects produced by the initial imperfection of a coupler and the existence of two-component parametric resonance to the vibration near the primary region of instability have not been studied yet.

In this study, an analytical method that determines the primary region of instability is developed and applied. The method of multiple time scales is employed to consider the steady state solutions and the occurrence of multi-component parametric resonance of the multi-degree-of-freedom dynamical system with time-dependent coefficients. Various effects, such as structural damping, geometric imperfection of a connecting rod, crank ratio, and piston mass ratio, to the response of a slider-crank mechanism are investigated. The occurrence of the growth of small amplitude vibration into large motion regime is also studied.

2. Basic formulas

As shown in Fig. 1, a slider-crank mechanism with an inextensible initially curved elastic coupler is considered. The mechanism consists of a rigid crank of radius r; an initially curved elastic coupler of length ℓ; and a frictionless piston of mass M.

From Fig. 1, the equations governing the motion of the system in the moving co-ordinate frame (*xyz* co-ordinates) can be derived from the dynamic equilibrium of forces and conservation of momenta and are given as

$$\mathbf{F}_{,s} = m\mathbf{R}_{,tt} + \hat{\mu}\mathbf{R}_{,t}, \quad 0 < s < \ell, t > 0, \tag{1a}$$

$$\bar{M}_{,s} + V = 0, \tag{1b}$$

$$\bar{M} = EIv_{,ss} \tag{1c}$$

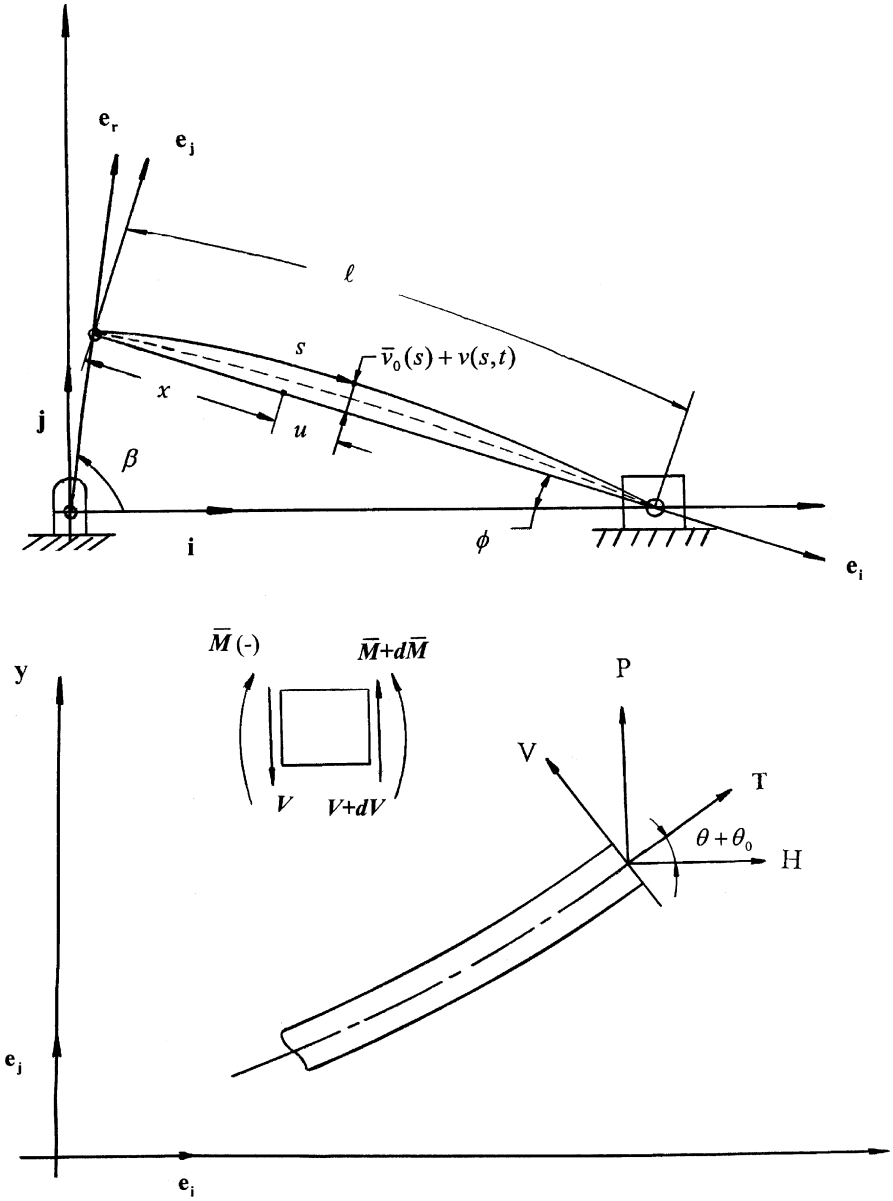

Fig. 1. System configuration and force equilibrium diagram.

with the inextensibility constraint $\mathbf{r}_{,s} \cdot \mathbf{r}_{,s} = 1$. The force $\mathbf{F}$ is given by

$$\begin{aligned}\mathbf{F} &= H\mathbf{e_i} + P\mathbf{e_j} \\ &= [(T\cos(\theta+\theta_0) - V\sin(\theta+\theta_0)]\mathbf{e_i} + [T\sin(\theta+\theta_0) + V\cos(\theta+\theta_0)]\mathbf{e_j}.\end{aligned} \tag{2}$$

In the above equations, $\bar{M}$ is the bending moment acting on the element; T and V are the axial and transverse forces in the coupler, respectively; $\hat{\mu}$ denotes damping coefficient; θ_0 and θ represent the initial angle between the neutral axis of the coupler and the x-axis and the dynamic angle from the static state, respectively; $\mathbf{e_i}$ and $\mathbf{e_j}$ represent the unit vectors of the moving co-ordinate (xyz co-ordinates) system whose x ($\mathbf{e_i}$) co-ordinate is along the centroidal line of the straight elastic link; m, E and I are the mass per unit length, Young's modulus and the area moment of inertia of the connecting rod, respectively; the subscript s and t denote the s and t differentiation. $\mathbf{R}(s,t)$ is the position vector of point s along the link at time t and has the form

$$\mathbf{R}(s,t) = r\mathbf{e_r} + \mathbf{r} = r\mathbf{e_r} + (x(s) + u(s,t))\mathbf{e_i} + (\bar{v}_0(s) + v(s,t))\mathbf{e_j}, \tag{3}$$

where $u(s,t)$ and $v(s,t)$ are the axial and transverse displacements of the rod from the dynamic undeformed state, respectively; $\mathbf{e_r}$ is the unit vector along the crank; $\bar{v}_0(s)$, $\bar{v}_0(s) = v_0^* \sin(\pi s/\ell)$, is the initial variation from straight axis with v_0^* being the amplitude of initial deviation. The relationship among $\mathbf{e_r}$, $\mathbf{e_i}$, $\mathbf{e_j}$, $\mathbf{i}$ and $\mathbf{j}$ are given by

$$\mathbf{e_r} = \cos(\beta+\phi)\mathbf{e_i} + \sin(\beta+\phi)\mathbf{e_j} = \cos\beta\mathbf{i} + \sin\beta\mathbf{j},$$

$$\mathbf{e_i} = \cos\phi\mathbf{i} + \sin\phi\mathbf{j},$$

$$\mathbf{e_j} = -\sin\phi\mathbf{i} + \cos\phi\mathbf{j},$$

where β is the angular displacement of the crank; $\mathbf{i}$ and $\mathbf{j}$ represent the unit vectors of the Cartesian frame in the plane of the mechanism. $\mathbf{R}_{,t}$ and $\mathbf{R}_{,tt}$ are the velocity and acceleration of points along the coupler in the moving coordinate system, respectively, and are obtained from

$$\begin{aligned}\mathbf{R}_{,t} = \frac{\mathrm{d}}{\mathrm{d}t}[\mathbf{R}(s,t)] &= [-r\beta_{,t}\sin(\beta+\phi) + u_{,t} + v_{,t}\phi_{,t} + (v+\bar{v}_0)\phi_{,t}]\mathbf{e_i} \\ &\quad + [r\beta_{,t}\cos(\beta+\phi) - (x+u)\phi_{,t} + v_{,t}]\mathbf{e_j} \equiv \dot{R}_x\mathbf{e_i} + \dot{R}_y\mathbf{e_j},\end{aligned} \tag{4}$$

$$\begin{aligned}\mathbf{R}_{,tt} = \frac{\mathrm{d}^2}{\mathrm{d}t^2}[\mathbf{R}(s,t)] &= [-r\beta_{,tt}\sin(\beta+\phi) - r\beta_{,t}^2\cos(\beta+\phi) + u_{,tt} - (x+u)\phi_{,t}^2 \\ &\quad - 2v_{,t}\phi_{,t} - (v+\bar{v}_0)\phi_{,tt}]\mathbf{e_i} + [r\beta_{,tt}\cos(\beta+\phi) - r\beta_{,t}^2\sin(\beta+\phi) + v_{,tt} \\ &\quad + (x+u)\phi_{,tt} + 2u_{,t}\phi_{,t} - (v+\bar{v}_0)\phi_{,t}^2]\mathbf{e_j} \equiv a_x\mathbf{e_i} + a_y\mathbf{e_j},\end{aligned} \tag{5}$$

where $\sin(\beta+\phi) \approx \sin\beta + \frac{1}{2}(r/\ell)\sin 2\beta - \frac{1}{2}(r/\ell)^2\sin^3\beta$ and $\cos(\beta+\phi) \approx \cos\beta - (r/\ell)\sin^2\beta - \frac{1}{2}(r/\ell)^2\cos\beta\sin^2\beta$. In addition, the angle ϕ and its time derivatives in the above equation can be eliminated from the following kinematic relationships [9]:

$$\begin{aligned}\sin\phi &= -\frac{r}{\ell}\sin\beta, \\ \phi_{,t} &= -\frac{r}{\ell}\beta_{,t}\cos\beta, \\ \phi_{,tt} &= \frac{r}{\ell}\beta_{,t}^2\sin\beta - \frac{r}{\ell}\beta_{,tt}\cos\beta.\end{aligned} \tag{6}$$

Substitution of Eqs. (1b) to (6) into Eq. (1a), the equations of motion in directions $\mathbf{e_i}$ and $\mathbf{e_j}$ yield

$$\{T[(1+u_{,s})-v_{,s}\bar{v}_{0,s}]+EIv_{,sss}(v_{,s}+\bar{v}_{0,s})\}_{,s}=\hat{\mu}\dot{R}_x+ma_x,\quad 0<s<\ell,\,t>0, \tag{7}$$

$$\{[T(v_{,s}+\bar{v}_{0,s})-EIv_{,sss}[(1+u_{,s})-v_{,s}\bar{v}_{0,s}]\}_{,s}=\hat{\mu}\dot{R}_y+ma_y,\quad 0<s<\ell,\,t>0, \tag{8}$$

where $\cos(\theta+\theta_0)\mathbf{i}+\sin(\theta+\theta_0)\mathbf{j}\approx[(1+u_{,s})-v_{,s}\bar{v}_{0,s}]\mathbf{i}+(v_{,s}+v_{0,s})\mathbf{j}$; $\dot{R}_x$, $\dot{R}_y$, $a_{x,}$ and a_y are defined by Eqs. (4) and (5). Therefore, Eq. (8) represents the motion of the linkage in the $\mathbf{e_j}$ direction and Eq. (7) determines the axial force $T(s,t)$ of the coupler.

In this study, two types of boundary conditions are considered. The first is that the coupler is assumed to be hinged at each end. Therefore, the longitudinal displacement vanishes at $s=0$. The moment and transverse displacement also vanish at $s=0,\ell$. The second is when Newton's second law is employed to provide a force balance between the axial and shear forces of the rod and the inertia force of the frictionless piston (e.g. Ref. [1]). The boundary conditions then are

$$u(0,t)=v(0,t)=v(\ell,t)=\frac{\partial^2 v(0,t)}{\partial s^2}=\frac{\partial^2 v(\ell,t)}{\partial s^2}=0, \tag{9}$$

$$(H+Ma_x)\cos\phi+(P+Ma_y)\sin\phi=0\quad\text{at } s=\ell. \tag{10}$$

Substitution of H and P in Eq. (2) into Eq. (10), it yields

$$\begin{aligned}&\{T[(1+u_{,s})-v_{,s}\bar{v}_{0,s}]+EIv_{,sss}(v_{,s}+\bar{v}_{0,s})+Ma_x\}\cos\phi\\&\quad-\{T(v_{,s}+\bar{v}_{0,s})-EIv_{,sss}[(1+u_{,s})-v_{,s}\bar{v}_{0,s}]+Ma_y\}\sin\phi=0\quad\text{at } s=\ell.\end{aligned} \tag{11}$$

Therefore, Eq. (11) determines the time dependent axial force at $s=\ell$, $T(\ell,t)$.

To determine the axial force $T(s,t)$, one integrates Eq. (7) and uses the boundary constraint, Eq. (11). After some manipulations, the result yields

$$T(s,t)\times[(1+u_{,s})-v_{,s}\bar{v}_{0,s}]+EIv_{,sss}(v_{,s}+\bar{v}_{0,s})=\int_0^s(\mu\dot{R}_x+ma_x)\,\mathrm{d}s+C(t), \tag{12}$$

where $C(t)$ is constant of integration and is given by

$$C(t)=T(\ell,t)\times[(1+u_{,s})-v_{,s}\bar{v}_{0,s}]|_{s=\ell}+EIv_{,sss}(v_{,s}+\bar{v}_{0,s})|_{s=\ell}-\int_0^\ell(\hat{\mu}\dot{R}_x+ma_x)\,\mathrm{d}s,$$

where $T(\ell,t)$ is able to be obtained from Eq. (11). This result now can be inserted into Eq. (8).

The equations of motion of the system with constant angular velocity, $\hat{\omega}=constant$, in dimensionless form can be obtained by introducing the following dimensionless quantities:

$$\begin{aligned}&\tau=\hat{\omega}t,\quad \hat{u}=\frac{u}{\ell},\quad \hat{v}=\frac{v}{\ell},\quad \hat{\bar{v}}_0=\frac{\bar{v}_0}{\ell},\quad \hat{\xi}=\frac{r}{\ell},\quad \eta=\frac{s}{\ell},\\&\hat{I}_m=\frac{EI}{m\ell^4\hat{\omega}^2},\quad \hat{I}_M=\frac{EI}{M\ell^3\hat{\omega}^2},\quad \hat{M}=\frac{M}{m\ell}.\end{aligned} \tag{13}$$

Substitution of Eq. (13) into Eq. (8), one gets

$$\begin{aligned}\hat{v}_{,\tau\tau} + \hat{I}_m \frac{\partial^4 \hat{v}}{\partial \eta^4} - \hat{\xi}^2(\cos^2\tau)(\hat{v} + \hat{\bar{v}}_0) - \frac{\partial T(\eta,\tau)}{\partial \eta}\frac{\partial v(\hat{v} + \hat{\bar{v}}_0)}{\partial \eta} - T(\eta,\tau)\frac{\partial^2(\hat{v} + \hat{\bar{v}}_0)}{\partial \eta^2} \\ - 2\hat{\xi}\cos\tau\hat{u}_{,\tau} + \hat{\xi}\sin\tau\hat{u} - \hat{\mu}\hat{v}_{,\tau} - \hat{\mu}\hat{\xi}\cos\tau\hat{u} \\ = \hat{\xi}\sin\tau(1-\eta) + \tfrac{1}{2}\hat{\xi}^2\sin 2\tau + \tfrac{1}{2}\hat{\xi}^3\sin^3\tau,\end{aligned} \tag{14}$$

where $\partial T(\eta,\tau)/\partial\eta$ and $T(\eta,\tau)$ are given in the appendix.

Now, the condition of small deformations is assumed. For this, one neglects the non-linear terms when compares these terms with the linear terms of $\hat{v}(\eta,\tau)$ and unit. The crank ratio $\hat{\xi}$ and the damping coefficient $\hat{\mu}$ are also assumed to be small quantities. Eq. (14) then becomes

$$\begin{aligned}\hat{v}_{,\tau\tau} + \hat{\mu}\hat{v}_{,\tau} + \hat{I}_m \frac{\partial^4 \hat{v}}{\partial \eta^4} + \hat{\xi}\cos\tau\frac{\partial(\hat{v} + \hat{\bar{v}}_0)}{\partial \eta} + \hat{\xi}\cos\tau[(\eta-1) - \hat{M}]\frac{\partial^2(\hat{v} + \hat{\bar{v}}_0)}{\partial \eta^2} \\ = \hat{\xi}\sin\tau(1-\eta) + \tfrac{1}{2}\hat{\xi}^2\sin 2\tau.\end{aligned} \tag{15}$$

Examination of the dynamics governed by Eq. (15) is the main aim in this study.

Representing $\hat{v}$ as continuous functions and letting

$$\hat{v} = \sum_{i=1}^{\infty} A_i(\tau)\sin i\pi\eta, \quad 0 < \eta < 1, \tau > 0. \tag{16}$$

The boundary condition, Eq. (9), then is satisfied. In the following, the Galerkin's method is to be applied to obtain the approximate solutions of the slider-crank mechanism. Following Galerkin's procedure for minimizing error, one substitutes Eq. (16) into Eq. (15) and multiplies Eq. (15) by $\sin j\pi\eta$ and integrates it with respect to η from zero to 1. The result yields

$$\begin{aligned}\ddot{A}_j(\tau) + \hat{\mu}\dot{A}_j(\tau) + [\omega_j^2 + \hat{\xi}\cos\tau(j\pi)^2(\hat{M}+1)]A_j(\tau) \\ + 2\hat{\xi}\cos\tau\sum_{i=1}^{\infty}(i\pi)\alpha_{ij}^{cs}A_i(\tau) - 2\hat{\xi}\cos\tau\sum_{i=1}^{\infty}(i\pi)^2\alpha_{ij}^{\eta ss}A_i(\tau) \\ = \frac{2}{j\pi}\hat{\xi}\sin\tau + \hat{\xi}\cos\tau[2\pi\alpha_{1j}^{\eta ss} - 2\pi\alpha_{1j}^{cs} - (\hat{M}+1)\pi^2\delta_{1j}]\hat{v}_0 \\ + \frac{2}{j\pi}[1-(-1)^j]\hat{\xi}^2\sin 2\tau, \quad \tau > 0,\ j = 1,2,3,\ldots,\ (\dot{}) = \frac{\mathrm{d}}{\mathrm{d}\tau},\end{aligned} \tag{17}$$

where $\omega_j^2 = (j\pi)^4\hat{I}_m$; $\hat{v}_0 = v_0^*/\ell$; δ_{ij} is the Kronecker delta symbol; α_{ij}^{cs} and $\alpha_{ij}^{\eta ss}$ are the integration of cosine and sine functions and are given in the appendix.

To analyze the system governed by Eq. (17), one allows the response of the system to be small but finite. Thus, the method of multiple time scales can be used to predict the responses of the system. According to this method, one assumes that the amplitude, $A_j(\tau)$, has the

expansion [10]

$$
\begin{aligned}
&A_j(\tau;\varepsilon) = \varepsilon A_{1j}(\tau_0,\tau_1,\tau_2,\ldots) + \varepsilon^2 A_{2j}(\tau_0,\tau_1,\tau_2,\ldots) + \varepsilon^3 A_{3j}(\tau_0,\tau_1,\tau_2,\ldots) + \cdots,\\
&\tau_n = \varepsilon^n \tau, \quad n = 0,1,2,\ldots,\\
&\frac{\mathrm{d}}{\mathrm{d}\tau} = \frac{\partial}{\partial\tau_0} + \varepsilon\frac{\partial}{\partial\tau_1} + \varepsilon^2\frac{\partial}{\partial\tau_2} + \cdots \equiv D_0 + \varepsilon D_1 + \varepsilon^2 D_2 + \cdots,\\
&\frac{\mathrm{d}^2}{\mathrm{d}\tau^2} \equiv D_0^2 + 2\varepsilon D_0 D_1 + \varepsilon^2(D_1^2 + 2D_0 D_2) + \cdots,
\end{aligned}
\tag{18}
$$

where ε is a measure of the amplitude of the response and is small compared to unity.

For the purpose of studying the parametric resonance of the differential equations, one substitutes Eq. (18) into Eq. (17) and sets $\hat{\xi} = \varepsilon\xi$, $\hat{v}_0 = \varepsilon v_0$ and $\hat{\mu} = \varepsilon\mu$. After manipulating these equations, one equates coefficients of equal power of ε and obtains to order one and two:

$$
\varepsilon^1: \quad D_0^2 A_{1j} + \omega_j^2 A_{1j} = \frac{2}{j\pi}\xi \sin\tau_0, \tag{19}
$$

$$
\begin{aligned}
\varepsilon^2: \quad D_0^2 A_{2j} + \omega_j^2 A_{2j} = &-\mu D_0 A_{1j} - 2D_0 D_1 A_{1j}\\
&- \xi\cos\tau_0\{(j\pi)^2(\hat{M}+1)A_{1j} + 2\sum_{i=1}^{\infty}(i\pi)[\alpha_{ij}^{cs} - (i\pi)\alpha_{ij}^{\eta ss}]A_{1i}\}\\
&- \xi\cos\tau_0 K_{1j} v_0 + \frac{1}{j\pi}[1-(-1)^j]\xi^2\sin 2\tau_0,
\end{aligned}
\tag{20}
$$

where $K_{1j} = [\pi^2(\hat{M}+1)\delta_{1j} + 2\pi\alpha_{1j}^{cs} - 2\pi^2\alpha_{1j}^{\eta ss}]$. It is shown in Eq. (19) that unbounded oscillation occurs when the frequency ω_j is 1. Therefore, in the following, the conditions considered are related to the cases when the natural frequency ω_j is not close to 1.

From Eq. (19), it is seen that the amplitude A_{1j} is harmonic in τ_0 and its solution can be represented as

$$
A_{1j} = a_j\cos(\omega_j\tau_0 + \phi_j) + \frac{2\xi}{(j\pi)(\omega_j^2 - 1)}\sin\tau_0 \equiv a_j\cos\beta_j + \xi\Lambda_j\sin\tau_0, \tag{21}
$$

where $a_j = a_j(\tau_1,\tau_2,\ldots)$ is the amplitude of response; $\phi_j = \phi_j(\tau_1,\tau_2,\ldots)$ is the phase angle and $\Lambda_j = 2/((j\pi)(\omega_j^2 - 1))$. Here, for convenience, rewriting Eq. (21) as

$$
\begin{aligned}
A_{1j} = &H_j(\tau_1,\tau_2,\ldots)\exp(\hat{\mathrm{i}}\omega_j\tau_0) + \bar{H}_j(\tau_1,\tau_2,\ldots)\exp(-\hat{\mathrm{i}}\omega_j\tau_0)\\
&- \hat{\mathrm{i}}\tfrac{1}{2}\hat{\xi}\Lambda_j(\exp(\hat{\mathrm{i}}\tau_0) - \exp(-\hat{\mathrm{i}}\tau_0)), \quad j = 1,2,3,\ldots,
\end{aligned}
\tag{22}
$$

where $\hat{\mathrm{i}} = \sqrt{-1}$ and $\bar{H}_j$ is the complex conjugate of H_j. $H_j = \frac{1}{2}a_j\exp(\hat{\mathrm{i}}\phi_j)$ with ϕ_j being the phase of the jth mode.

To seek the solution of A_{2j} defined by Eq. (20), one substitutes Eq. (21) into Eq. (20). After some manipulations, the result yields

$$D_0^2 A_{2j} + \omega_j^2 A_{2j} = \mu a_j \omega_j \sin\beta_j + 2\omega_j[(D_1 a_j)\sin\beta_j + a_j(D_1\phi_j)\cos\beta_j - \xi\left\{\tfrac{1}{2}(j\pi)^2(\hat{M}+1)a_j(\cos\beta_{1j}^{+} + \cos\beta_{1j}^{-}) + \sum_{i=1}^{\infty}[(i\pi)\alpha_{ij}^{cs} - (i\pi)^2\alpha_{ij}^{\eta ss}] \times a_i(\cos\beta_{1i}^{+} + \cos\beta_{1i}^{-})\right\} - \xi K_{1j} v_0 \cos\tau - \xi^2\left\{\tfrac{1}{2}(j\pi)^2(\hat{M}+1)\Lambda_j + \sum_{i=1}^{\infty}[(i\pi)\alpha_{ij}^{cs} - (i\pi)^2\alpha_{ij}^{\eta ss}]\Lambda_i - \frac{1}{j\pi}[1-(-1)^j]\right\}\sin 2\tau_0, \tag{23}$$

where $\beta_{1j}^{+} = (\omega_j + 1)\tau_0 + \phi_j$ and $\beta_{1j}^{-} = (\omega_j - 1)\tau_0 + \phi_j$.

It is known that a multi-degree-of-freedom dynamic system with parametric excitation will experience multi-components parametric resonance when two or more internal frequencies and the excitation frequency are commensurable or nearly commensurable. For a dynamic system with finite degrees of freedom similar to that defined by Eq. (23), parametric resonance may exist when $\omega_m \approx \frac{1}{2}$, $\omega_n - \omega_m \approx 1$ $(n > m)$. Here ω_m is the dimensionless internal frequency of the mth mode of vibration.

In order to express the commensurable relations of ω_m to $\frac{1}{2}$ and $\omega_n - \omega_m$ to 1, the detuning parameters σ_m and σ_{mn} are introduced:

$$\tfrac{1}{2} = \omega_m + \varepsilon\sigma_m, \tag{24}$$

$$1 = \omega_n - \omega_m + \varepsilon\sigma_{mn}, \tag{25}$$

where $\omega_n = (n/m)^2\omega_m$. The relationship between σ_m and σ_{mn} can be determined from Eqs. (24) and (25) which yields

$$\varepsilon\sigma_{mn} = \left[3 - \left(\frac{n}{m}\right)^2\right]\omega_m + 2\varepsilon\sigma_m \equiv B_{mn}\omega_m + 2\varepsilon\sigma_m. \tag{26}$$

Further, multiplying Eq. (25) by τ_0, it yields

$$\tau_0 = \left[1 - \left(\frac{m}{n}\right)^2\right]\omega_n\tau_0 + \varepsilon\sigma_{mn}\tau_0 \equiv \bar{B}_{mn}\omega_n\tau_0 + \varepsilon\sigma_{mn}\tau_0. \tag{27}$$

From Eq. (27), one finds that if $\bar{B}_{mn}$ is near 1 the resonance occurs in the nth mode of vibration. For this, one sets $\bar{B}_{mn} = 1 + \varepsilon\hat{\sigma}_{mn}$.

Returning to Eq. (23), for the sums and differences of the arguments of the cosine and sine functions of unequal arguments one has

$$\beta_{1m}^{-} = (\omega_m - 1)\tau_0 + \phi_m = -(\omega_m\tau_0 + \phi_m) - 2(\sigma_m\tau_1 - \phi_m) \equiv -(\beta_m + 2\delta_m), \tag{28}$$

$$\beta_{1m}^{+} = (\omega_m + 1)\tau_0 + \phi_m = (\omega_n\tau_0 + \phi_n) + (\sigma_{mn}\tau_1 + \phi_m - \phi_n) \equiv \beta_n + \delta_{mn}, \tag{29}$$

$$\beta_{1n}^{-} = (\omega_n - 1)\tau_0 + \phi_n = (\omega_m\tau_0 + \phi_m) - (\sigma_{mn}\tau_1 + \phi_m - \phi_n) = \beta_m - \delta_{mn}, \tag{30}$$

$$\tau_0 = (\omega_m + 1)\tau_0 + \phi_m = (\omega_n\tau_0 + \phi_n) + (\sigma_{mn}^{*}\tau_1 - \phi_n) \equiv \beta_n + \delta_{mn}^{*}, \tag{31}$$

where $\delta_m = \sigma_m\tau_1 - \phi_m$, $\delta_{mn} = \sigma_{mn}\tau_1 + \phi_m - \phi_n$, and $\delta^*_{mn} = (\hat{\sigma}_{mn}\omega_n + \sigma_{mn})\tau_1 - \phi_n \equiv \sigma^*_{mn}\tau_1 - \phi_n$. Therefore $\delta_m = \delta_m(\tau_1, \tau_2, \ldots)$, $\delta_{mn} = \delta_{mn}(\tau_1, \tau_2, \ldots)$ and $\delta^*_{mn} = \delta^*_{mn}(\tau_1, \tau_2, \ldots)$ are three new phase angles. From the definition of σ_m and σ_{mn} one has

$$D_1\phi_m = \sigma_m - D_1\delta_m \quad \text{and} \quad D_1\phi_n = \sigma_{mn} + D_1\phi_m - D_1\delta_{mn}. \tag{32}$$

Returning to Eq. (23) the solvability conditions are the vanishing of the secular terms. These are, in complex form:

$$4\omega_m\hat{\mathrm{i}}\left(D_1H_m + \tfrac{1}{2}\mu H_m\right) + 2\xi f^*_{mm}\bar{H}_m\exp(2\hat{\mathrm{i}}\sigma_m\tau_1) - 2\xi f_{nm}H_n\exp(-\hat{\mathrm{i}}\sigma_{mn}\tau_1) = 0, \tag{33}$$

$$4\omega_n\hat{\mathrm{i}}(D_1H_n + \tfrac{1}{2}\mu H_n) + 2\xi f_{mn}H_m\exp(\hat{\mathrm{i}}\sigma_{mn}\tau_1) = -2\xi K_{1n}v_0\exp(\hat{\mathrm{i}}\sigma^*_{mn}\tau_1), \tag{34}$$

where $f^*_{mm} = \frac{1}{2}(m\pi)^2(\hat{M}+1) + f_{mm}$ and $f_{nm} = [(n\pi)\alpha^{cs}_{nm} - (n\pi)^2\alpha^{\eta ss}_{nm}]$.

The main purpose of Eqs. (33) and (34) is to determine the response of motion in steady state and regions of instability.

To determine the solutions and correspondingly the local stability of parametric resonance one follows the procedure outlined in Ref. [10] and lets

$$H_k = \tfrac{1}{2}(x_k - \hat{\mathrm{i}}z_k)\exp(\hat{\mathrm{i}}\theta_k\tau_1), \quad k = m, n. \tag{35}$$

Here x_k and z_k are real and $\theta_k = \mathrm{d}\phi_k/\mathrm{d}\tau_1$.

For the resonant condition, one substitutes Eq. (35) into the resonant equations defined by Eqs. (33) and (34) and separates the real and imaginary parts. The result yields

$$x'_m + \tfrac{1}{2}\mu x_m + \left(\theta_m + \frac{\xi}{2\omega_m}f^*_{mm}\right)z_m - \frac{\xi}{2\omega_m}f_{nm}z_n = 0, \tag{36}$$

$$z'_m + \tfrac{1}{2}\mu z_m + \left(-\theta_m + \frac{\xi}{2\omega_m}f^*_{mm}\right)x_m + \frac{\xi}{2\omega_m}f_{nm}x_n = 0, \tag{37}$$

$$x'_n + \tfrac{1}{2}\mu x_n + \theta_n z_n - \frac{\xi}{2\omega_n}f_{mn}z_m = 0, \tag{38}$$

$$z'_n + \tfrac{1}{2}\mu z_n - \theta_n\hat{x}_n + \frac{\xi}{2\omega_n}f_{mn}x_m = -\frac{\xi}{2\omega_n}K_{1n}v_0, \tag{39}$$

where $(\ )' = \mathrm{d}/\mathrm{d}\tau_1$.

The local stability of a fixed point with respect to a small perturbation for each resonant case hence can be determined by the eigenvalues λ which are given by the zero of the determinant of the perturbation equations. For this, a small perturbation is superimposed on x_k and z_k $(k = m, n)$ and one has

$$x_k = x^0_k + \hat{x}_k \text{ and } z_k = z^0_k + \hat{z}_k. \tag{40}$$

Here $x^0_k, z^0_k, \hat{x}_k$ and $\hat{z}_k$ are the fixed points and the disturbances, respectively. The determinant of the perturbation equations can be obtained by substituting Eq. (40) into Eqs. (36)–(39).

The result yields

$$\begin{vmatrix} \hat{\lambda} & \theta_m + \frac{\xi}{2\omega_m} f^*_{mm} & 0 & -\frac{\xi}{2\omega_m} f_{nm} \\ -\theta_m + \frac{\xi}{2\omega_m} f^*_{mm} & \hat{\lambda} & \frac{\xi}{2\omega_m} f_{nm} & 0 \\ 0 & -\frac{\xi}{2\omega_n} f_{mn} & \hat{\lambda} & \theta_n \\ \frac{\xi}{2\omega_n} f_{mn} & 0 & -\theta_n & \hat{\lambda} \end{vmatrix} = 0, \tag{41}$$

where $\hat{\lambda} = \lambda + \frac{1}{2}\mu$, $\theta_m = D_1\phi_m = \sigma_m$, and $\theta_n = D_1\phi_n = \sigma_m + \sigma_{mn}$. Thus, the characteristic equation of Eq. (41) has the form

$$\hat{\lambda}^4 + r_2\hat{\lambda}^2 + r_4 = 0, \tag{42}$$

where

$$\begin{aligned} r_2 &= \sigma_m^2 + (\sigma_m + \sigma_{mn})^2 - \left(\frac{\xi}{2\omega_m} f^*_{mm}\right)^2 + \frac{\xi^2}{2\omega_m\omega_n} f_{mn} f_{nm}, \\ r_4 &= \left[\sigma_m(\sigma_m + \sigma_{mn}) - \frac{\xi^2}{4\omega_m\omega_n} f_{mn} f_{nm}\right]^2 - \left[\frac{\xi}{2\omega_m} f^*_{mm}(\sigma_m + \sigma_{mn})\right]^2. \end{aligned} \tag{43}$$

The root of Eq. (42) is

$$\lambda = -\tfrac{1}{2}\mu \pm \sqrt{\tfrac{1}{2}[-r_2 \pm \sqrt{r_2^2 - 4r_4}]}.$$

It is known that the stability of response determines the existence of steady state reaction. Hence, boundaries of stable and unstable solutions have to be determined. Those are given as follows:

1. For the condition when $r_2 > 0$:
   - 1.1. In the case when $\sqrt{r_2^2 - 4r_4} > r_2$, the steady state solutions are stable if $\sqrt{\frac{1}{2}[-r_2 \pm \sqrt{r_2^2 - 4r_4}]} < \mu/2$ and unstable if $\sqrt{\frac{1}{2}[-r_2 \pm \sqrt{r_2^2 - 4r_4}]} > \mu/2$.
   - 1.2. For the case when $\sqrt{r_2^2 - 4r_4} < r_2$, the responses are stable.
2. For the condition when $r_2 < 0$:
   - 2.1. The steady state solutions are unstable if $\sqrt{r_2^2 - 4r_4} > 0$.
   - 2.2. For the case when $\sqrt{r_2^2 - 4r_4} < 0$, the steady state solutions are stable if $\sqrt{\frac{1}{2}[-r_2 \pm \sqrt{r_2^2 - 4r_4}]} < \mu/2$ and unstable if $\sqrt{\frac{1}{2}[-r_2 \pm \sqrt{r_2^2 - 4r_4}]} > \mu/2$.

The transition curves and steady state responses of the system corresponding to conditions 1 and 2 then can be obtained and are summarized as follows:

Case 1: *For the state when* $r_2 \neq 0$ *and* $\mu \neq 0$. In this case, the steady state solutions of the system are

$$a_m = \frac{2(\xi/\omega_m)K_{1n}v_0}{\Delta_1}\sqrt{\mu^4 + \Gamma_1\mu^2 + \Gamma_2}, \tag{44}$$

$$a_n = \frac{2K_{1n}v_0}{\Delta_1}\sqrt{\mu^6 + \Gamma_1^*\mu^4 + \Gamma_2^*\mu^2 + \Gamma_3^*}, \tag{45}$$

where $\Delta_1 = \mu^4 + 4r_2\mu^2 + 16r_4$; $K_{1n} = [\pi^2(\hat{M}+1)\delta_{1n} + 2\pi\alpha_{1n}^{cs} - 2\pi^2\alpha_{1n}^{\eta ss}]$; r_2 and r_4 are given by Eq. (43); $\Gamma_1, \Gamma_2, \Gamma_1^*, \Gamma_2^*$, and Γ_3^* are given in the appendix.

It is observed from Eq. (44) that the growth of small amplitude of vibrations into large amplitude regime occurs if the denominator Δ_1 is close to zero and unbounded solutions exist if $\Delta_1 = 0$. In other words, the steady state response of the system may become large amplitude vibrations even if the geometric imperfection of the coupler is tiny.

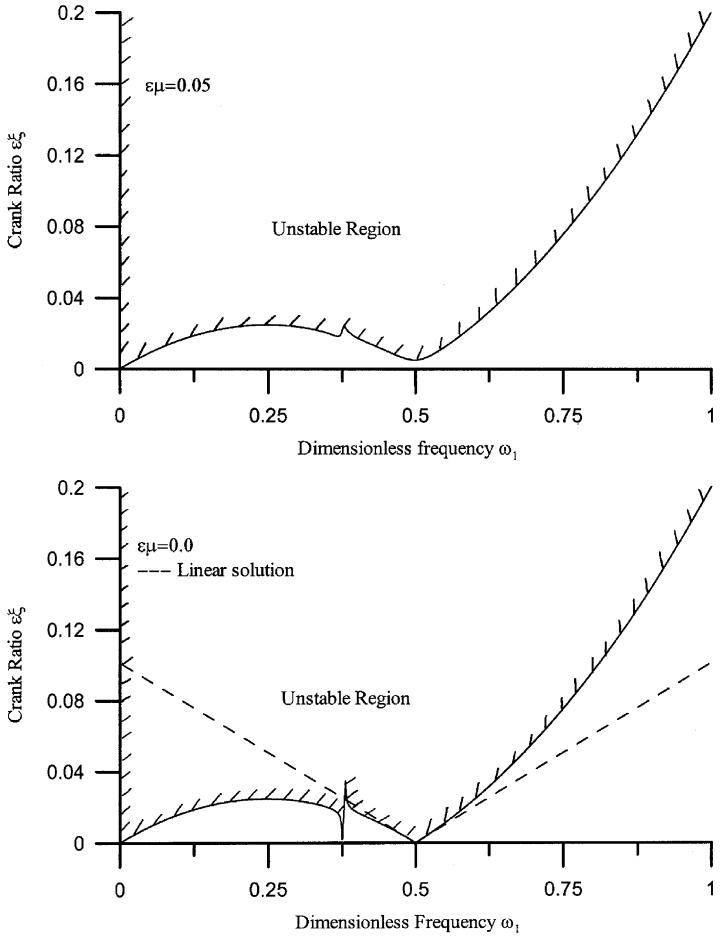

Fig. 2. Transition curves emanating from $\omega_1 = 0.5$ and $\omega_2 = 4\omega_1$ in the $\varepsilon\xi$–ω plane for $\hat{M} = 0.5$ and $\varepsilon\mu = 0$ (lower plot) and $\varepsilon\mu = 0.05$ (upper plot).

Returning to the stability analysis, the transition values that separate the stable and unstable motion of the steady state response are $\sqrt{\frac{1}{2}[-r_2 \pm \sqrt{r_2^2 - 4r_4}]} = \mu/2$ or

$$\mu^4 + 4r_2\mu^2 + 16r_4 = 0. \tag{46}$$

Note that Eq. (46) is the same result as Δ_1 defined by Eq. (44). From Eq. (44), it is observed that unbounded solutions exist if $\Delta_1 = 0$ and the growth of small amplitude of vibrations into large motion regime occurs if the denominator Δ_1 is close to zero. Hence, the transition curves that separate unbounded and bounded solutions are determined by $\Delta_1 = 0$. Multiplying Eq. (46) by ε^4

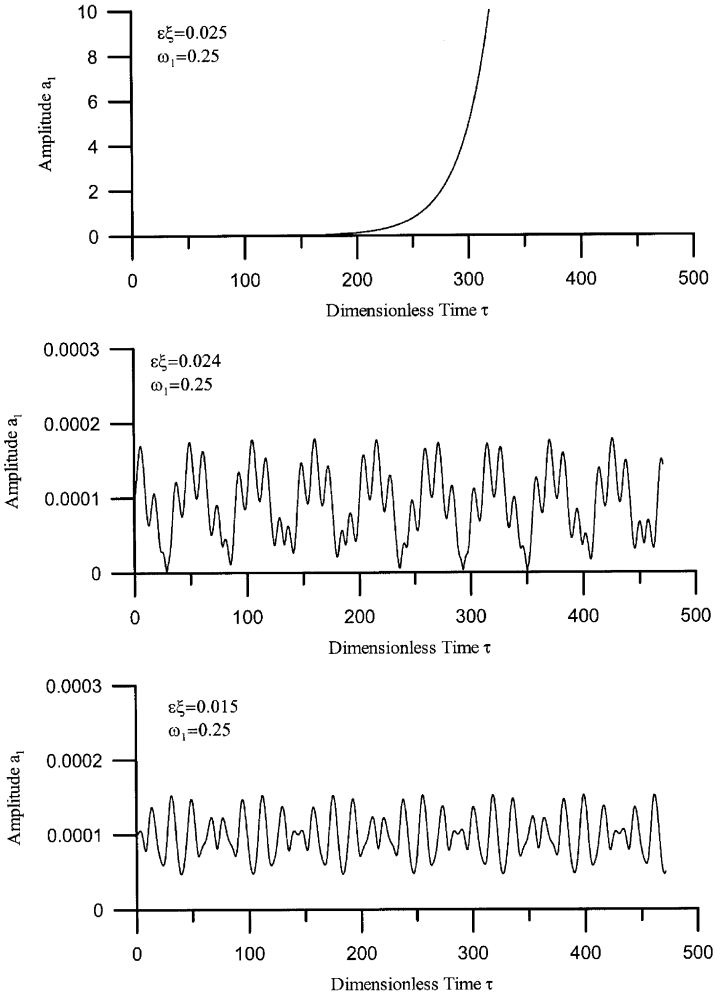

Fig. 3. Time history of the amplitude a_1 for $\hat{M} = 0.5$, $\omega_1 = 0.25$ and three different values of the crank ratio $\varepsilon\xi$, $\varepsilon\xi = 0.015$ (bottom plot), 0.024 (middle one), and 0.025 (top plot).

and substituting Eq. (26) with Eqs. (24) and (25) to eliminate $\varepsilon\sigma_{mn}$ in Eq. (46), the result yields

$$\varepsilon^4(\mu^4+4r_2\mu^2+16r_4)=\left(\frac{f_{mn}f_{nm}}{(n/m)^2\omega_m^2}\right)^2(\varepsilon\xi)^4-\left\{(\varepsilon\mu)^2\left[\left(\frac{f_{mm}^*}{\omega_m}\right)^2-2\frac{f_{mn}f_{nm}}{(n/m)^2\omega_m^2}\right]+8(\varepsilon\sigma_m)(K_{mn}\omega_m+3\varepsilon\sigma_m)\left(\frac{f_{mn}f_{nm}}{(n/m)^2\omega_m^2}\right)+4\left[\frac{f_{mm}^*}{\omega_m}(K_{mn}\omega_m+3\varepsilon\sigma_m)\right]^2\right\}(\varepsilon\xi)^2+\{(\varepsilon\mu)^4+4(\varepsilon\mu)^2[(\varepsilon\sigma_m)^2+(K_{mn}\omega_m+3\varepsilon\sigma_m)]+16(\varepsilon\sigma_m)^2(K_{mn}\omega_m+3\varepsilon\sigma_m)^2\}=0. \quad (47)$$

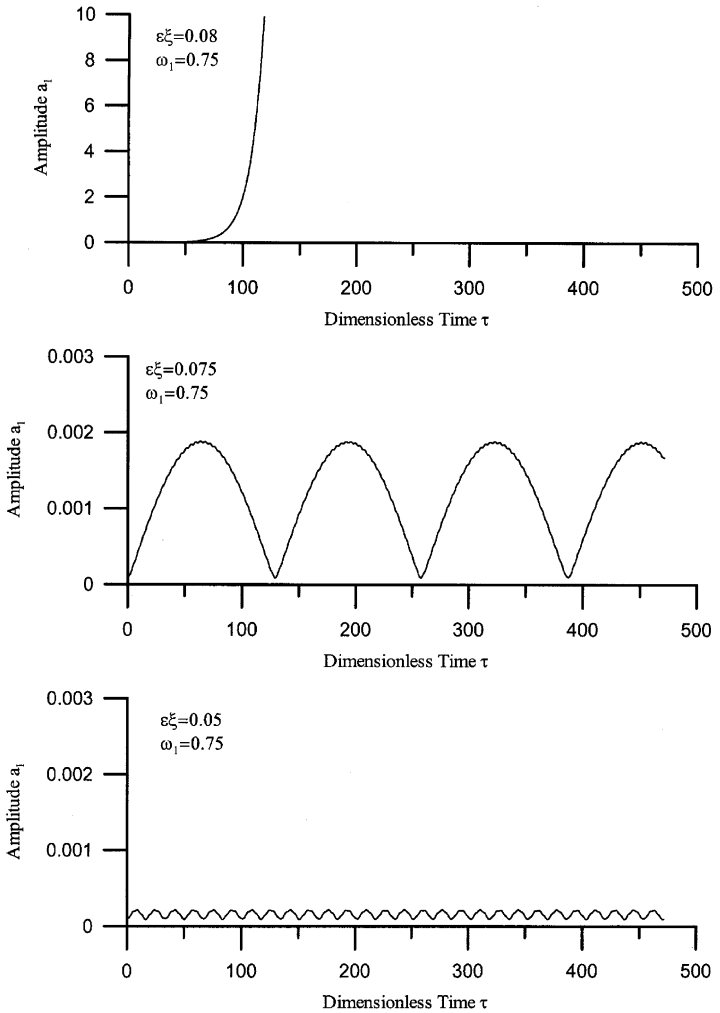

Fig. 4. Time history of the amplitude a_1 for $\hat{M}=0.5$, $\omega_1=0.75$ and three different values of the crank ratio $\varepsilon\xi$, $\varepsilon\xi=0.05$ (bottom plot), 0.075 (middle one), and 0.08 (top plot).

In the above equation, $\varepsilon\xi$ is the crank ratio and has to be no less than zero. Therefore, the positive roots of Eq. (47) of $\varepsilon\xi$ imply the existence of transition values.

Case 2: *For the state when* $r_2 \neq 0$ *and* $\mu = 0$. In this case, the steady state solutions of the system are

$$a_m = \left(\frac{\xi}{8\omega_m}\right)\frac{K_{1n}v_0}{r_4}\sqrt{\Gamma_2}, \tag{48}$$

$$a_n = \frac{K_{1n}v_0}{8r_4}\sqrt{\Gamma_3^*}. \tag{49}$$

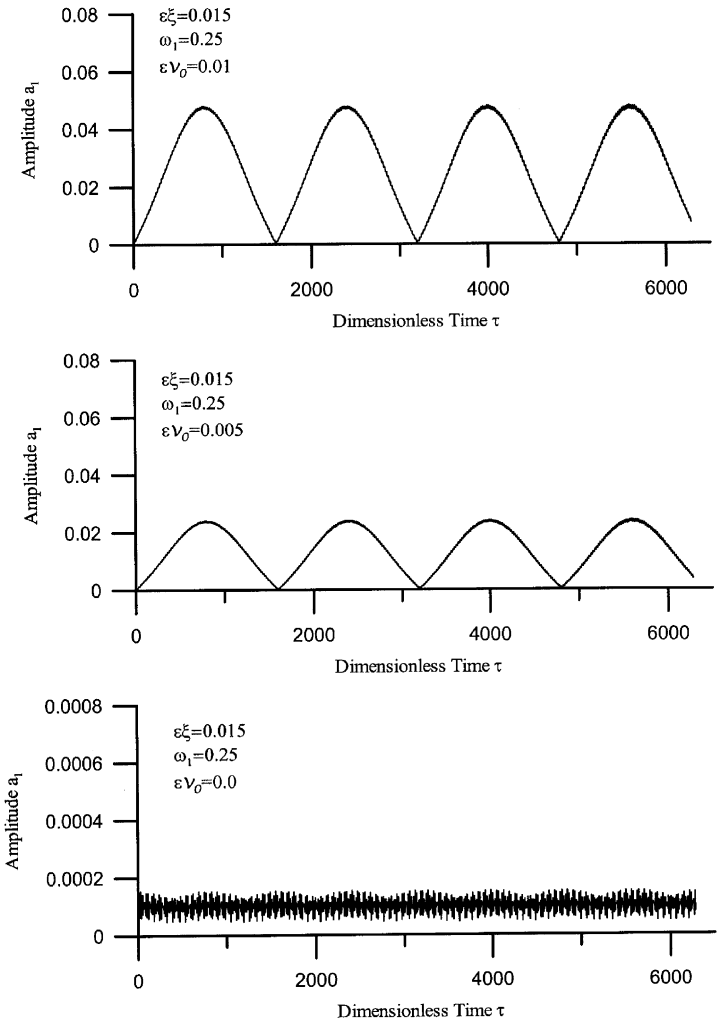

Fig. 5. Time history of the amplitude a_1 for $\hat{M} = 0.5$, $\omega_1 = 0.25$ and $\varepsilon\xi = 0.015$. Three different values of dimensionless amplitude of geometric imperfection of a connecting rod εv_0 are selected. Those are $\varepsilon v_0 = 0.0$ (geometric perfect, bottom plot), 0.005 (middle one), and 0.01 (top plot).

Similar as previous case, the growth of small amplitude of vibrations into large amplitude motion occurs if the denominator r_4 is near zero and unbounded solutions exist if $r_4 = 0$.

The transition values that divide the stable and unstable motion of the steady state solution are $r_4 = 0$ or

$$\sigma_m(\sigma_m + \sigma_{mn}) - \frac{\xi^2}{4\omega_m\omega_n} f_{mn}f_{nm} = \pm\frac{\xi}{2\omega_m} f^*_{mm}(\sigma_m + \sigma_n). \tag{50}$$

Similar to that done in Case 1, multiplying Eq. (50) by ε^2 and substituting Eq. (26) with Eqs. (24) and (25) to eliminate $\varepsilon\sigma_{mn}$ in Eq. (50), the result yields

$$\frac{f_{mn}f_{nm}}{4(n/m)^2\omega_m^2}(\varepsilon\xi)^2 \pm \frac{f^*_{mm}}{2\omega_m}(K_{mn}\omega_m + 3\varepsilon\sigma_m)(\varepsilon\xi) - \varepsilon\sigma_m(K_{mn}\omega_m + 3\varepsilon\sigma_m) = 0. \tag{51}$$

Therefore, the positive roots of Eq. (51) of $\varepsilon\xi$ represent the existence of transition values.

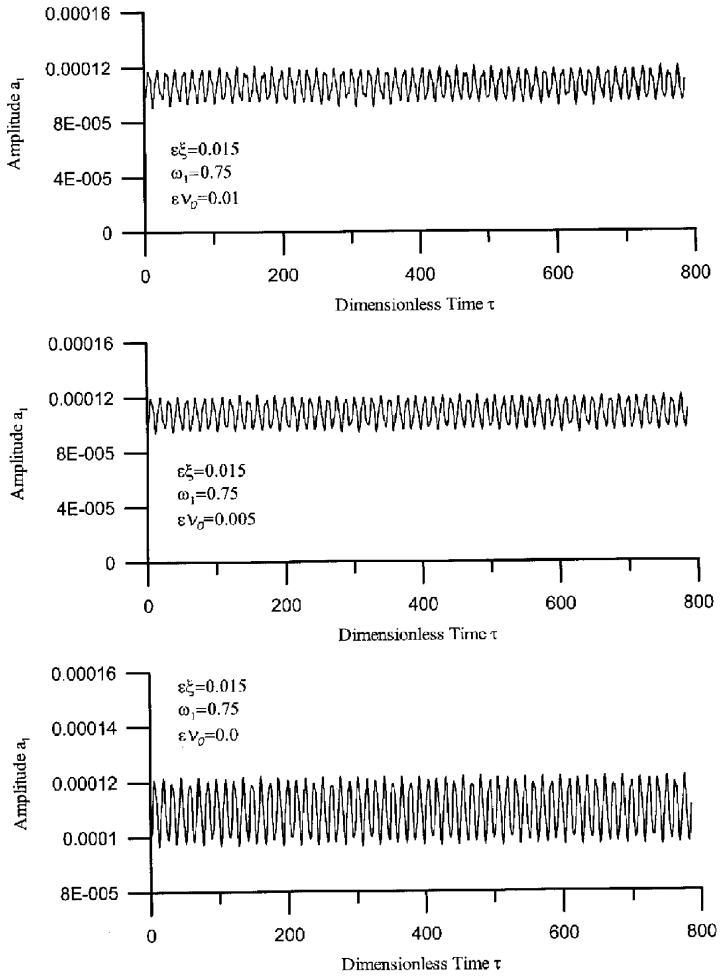

Fig. 6. Time history of the amplitude a_1 with the same parameters as used in Fig. 5, except $\omega_1 = 0.75$.

It is mentioned here that in the absence of internal resonance, $K_{mn} = f_{mn} = f_{nm} = 0$, Eq. (51) reduces to the result of Badlani and Midha [1] for $\omega_m \cong \frac{1}{2}$. That is, they reduce to

$$\varepsilon\sigma_m = \pm \frac{\varepsilon\xi f_{mm}}{2\omega_m} = \pm \frac{\varepsilon\xi}{2\omega_m}\left[\tfrac{1}{2}(m\pi)^2\left(\hat{M} + \tfrac{1}{2}\right)\right]. \tag{52}$$

3. Numerical results and discussions

Without loss of generality and considering the commensurable relations among frequencies and the probability of occurrence in nature, for the case of $\omega_m \cong \frac{1}{2}$ and $\omega_n - \omega_m \cong 1$, one chose $m = 1$

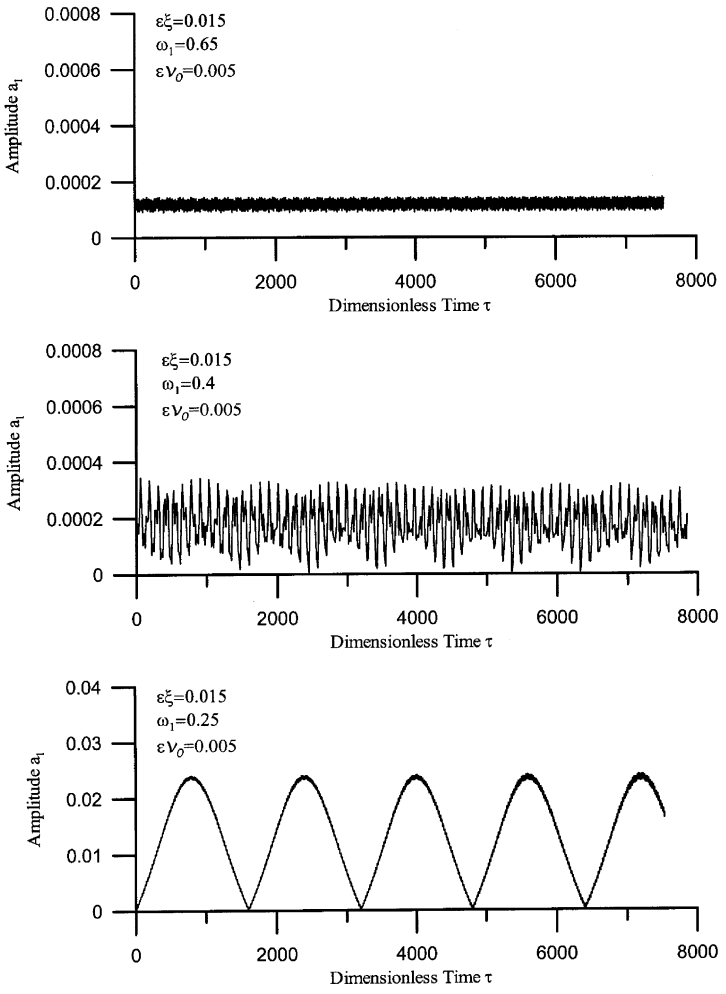

Fig. 7. Time history of the amplitude a_1 for $\hat{M} = 0.5$, $\varepsilon\xi = 0.015$, $\varepsilon v_0 = 0.005$, and three different values of the fundamental frequency ω_1, $\omega_1 = 0.25$ (lowest plot), 0.4 (middle one) and 0.65 (top plot).

and $n = 2$ to present the basic characteristics of the occurrence of two-component parametric resonance. It is recalled that the parameter $\varepsilon\xi$ is the crank ratio. ω_j is the dimensionless natural frequency and is defined by $\omega_j = (j\pi)^2\sqrt{EI/(ml^4\hat{\omega}^2)}$, where $\hat{\omega}$ is the constant angular velocity of the crank.

In addition to the stability analysis, the existence of perturbation solutions is verified by numerically integrating the modulation equations, Eqs. (36)–(39), by the Runge–Kutta method.

Fig. 2 presents the transition curves that separate the regions of bounded and unbounded (shaded area) motions emanating from $\omega_1 = \frac{1}{2}$ and $\omega_2 = 4\omega_1$ in the $\varepsilon\xi$–ω parameter plane for $\hat{M} = 0.5$, and $\varepsilon\mu = 0$ (lower plot) and $\varepsilon\mu = 0.05$ (upper plot). The solid and dash lines denote the transient curves for the first mode of vibration under the condition of two- and one-component parametric resonances, respectively. From this figure, one finds that there exists only minor

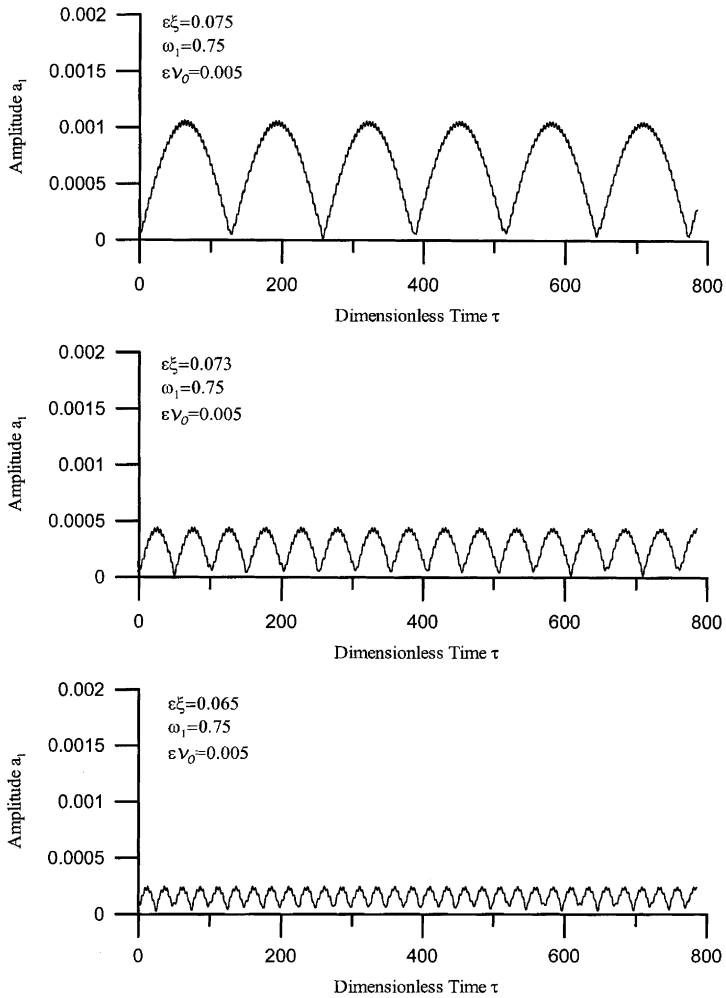

Fig. 8. Time history of the amplitude a_1 for $\hat{M} = 0.5$, $\omega_1 = 0.75$, $\varepsilon v_0 = 0.005$, and three different values of the crank ratio $\varepsilon\xi$, $\varepsilon\xi = 0.065$ (lowest plot), 0.0.073 (middle one) and 0.075 (top plot).

difference between zero and non-zero values of $\varepsilon\mu$. Hence, the coefficient of damping $\varepsilon\mu$ used in the numerical examples, unless otherwise specified, is set to be zero.

This figure also shows that if the natural frequency ω_1 is smaller than one-half of the excitation frequency, the occurrence of two-component parametric resonance enlarges the region of instability when compares it with the region of instability produced by one-component parametric resonance. In other words, unstable motion may occur even if the fundamental frequency is far less than the excitation frequency when there exists the occurrence of two-component parametric resonance. This is, perhaps, due to the variation of energy between modes and is not found in the

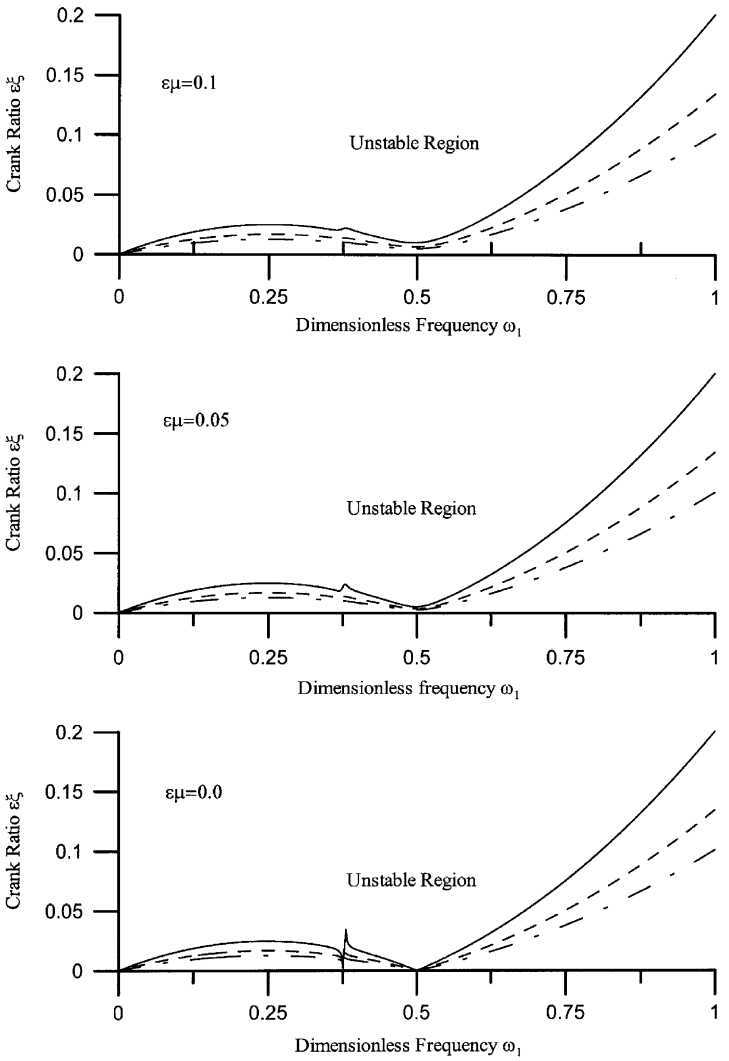

Fig. 9. Transition curves emanating from $\omega_1 = 0.5$ and $\omega_2 = 4\omega_1$ in the $\varepsilon\xi$–ω plane for $\hat{M} = 0.5$ (solid lines), 1.0 (dash lines), and 1.5 (chain dot lines). Three different values of damping coefficients are selected, $\varepsilon\mu = 0$ (lower plot) , $\varepsilon\mu = 0.05$ (middle one), and $\varepsilon\mu = 0.1$ (top plot).

condition of one-component parametric resonance. The validity of the model is verified by numerically integrating the modulation equations. The results are shown in Figs. 3 and 4.

Fig. 3 shows the long-time behavior of the amplitude a_1 for $\omega_1 = 0.25$ with three different values of crank ratio, $\varepsilon\xi = 0.015$ (bottom plot), $\varepsilon\xi = 0.024$ (middle one), and $\xi = 0.025$ (top plot). Fig. 4 illustrates similar information to that shown in Fig. 3, except in this figure ω_1 is set to be 0.075. In addition, three different values of crank ratio $\varepsilon\xi$ are selected. Those are $\varepsilon\xi = 0.05$ (lowest one), 0.075 (middle plot), and 0.08 (top one). These two figures clearly show the existence of bounded (stable) and unbounded (unstable) solutions.

In the following numerical examples, various effects produced by the variation of parameters, such as geometric imperfection of a coupler, detuning parameter of frequency, crank ratio, and piston mass ratio, to the response of the system are taken into account and studied.

Fig. 5 shows the time history of the amplitude a_1 for $\hat{M} = 0.5$, $\varepsilon\sigma_1 = 0.25$ ($\omega_1 = 0.25$), and $\varepsilon\xi = 0.015$. In this figure, three different values of initial imperfection of the coupler are chosen, which are $\varepsilon v_0 = 0.0$ (initial straight, lowest plot), $\varepsilon v_0 = 0.005$ (middle one), and $\varepsilon v_0 = 0.01$ (top plot). Fig. 6 presents similar information to that shown in Fig. 5, except in this figure $\varepsilon\sigma_1 = -0.25$ ($\omega_1 = 0.75$).

From these two figures, it is observed that under the condition when the fundamental frequency is small, for example $\omega_1 = 0.25$ (Fig. 5), the geometric imperfection of a coupler plays an important role to the amplitude of response. In general, the initial curvature of a linkage amplifies the amplitude of vibration. However, the magnification of the amplitude in response decreases with the increase of fundamental frequency, as shown in Fig. 6 ($\omega_1 = 0.75$). This is expected since from Eqs. (33) and (34), one finds that the amplitude of response decreases as the frequency increases. It is also evident in Fig. 7.

Fig. 7 shows the long-time behavior of the amplitude a_1 for $\varepsilon\xi = 0.015$ and $\varepsilon v_0 = 0.005$. Three different values of fundamental frequency are chosen, which are $\omega_1 = 0.25$ (bottom plot), 0.4 (middle one), and 0.65 (top plot). It clearly indicates that the magnification in response produced by the geometric imperfection of a connecting rod decreases with the increase of the frequency.

As shown in Eq. (44), unbounded solution occurs if the denominator $\Delta_1 = 0$ and the growth of small amplitude of vibration exists if the denominator Δ_1 is close to zero. In other words, unbounded solutions exist if the vibrations take place in the region of instability, including at transient values. The enlargement of small amplitude of vibrations into large motion regime occurs if the vibrations arise near the boundary of stable region.

Fig. 8 illustrates the time history of the amplitude a_1 for $\hat{M} = 0.5$, $\varepsilon v_0 = 0.005$, and $\omega_1 = 0.75$. Three different values of crank ratio are used. Those are $\varepsilon\xi = 0.065$ (lowest plot), 0.073 (middle one), and 0.075 (top plot). It evidently indicates the growth of small amplitude of vibration into large motion occurs if the oscillation takes place near the transient values.

The transition curves emerging from $\omega_1 = \frac{1}{2}$ and $\omega_2 = 4\omega_1$ in the $\varepsilon\xi$–ω parameter plane for different values of $\hat{M}$ and $\varepsilon\mu$ are shown in Fig. 9. The values of $\hat{M}$ used are 0.5 (solid lines), 1.0 (dash lines), and 1.5 (chain dot lines). The values of $\varepsilon\mu$ selected are 0.0 (bottom plot), 0.05 (middle one), and 0.1 (top plot). The result shows that the increase of piston mass ratio enlarges the region of instability. In addition, it is interesting to find that under the condition when $\varepsilon\mu = 0$, there exist two values of detuning parameters ($\varepsilon\sigma_1 = 0.0$ and 0.125) such that the motion of the system is fully unstable.

4. Conclusions

In this study, the mechanics of a slider-crank mechanism and the weak form of the occurrence of two-component parametric resonance are obtained. The growth of small amplitude of vibration into large motion regime is studied. Various effects, such as the existence of two-component parametric resonance, piston mass ratio, crank ratio, and initial imperfection of a coupler, to the response of the system are also investigated.

Result of the study shows that under the condition of two-component parametric resonance, the excitation created by the geometric imperfection of a coupler can result significant effects to the vibrations of the system near the primary region of instability. This is due to the interaction of energy between modes and cannot be observed in the case of one-component parametric resonance. The result also indicates that the magnification in response decreases as the fundamental frequency increases. In addition, the growth of small amplitude vibration into large motion regime occurs if the vibrations arise close to the boundary of stable region.

Appendix

$$\frac{\partial T(\eta,\tau)}{\partial \eta} \approx -\hat{\xi}\cos\tau + \hat{\xi}^2\sin^2\tau - \hat{\xi}^2\eta\cos^2\tau + 2\hat{\xi}\hat{v}_{,\tau}\cos\tau - \hat{\xi}(\hat{v}+\hat{v}_0)\sin\tau + \tfrac{1}{2}\hat{\xi}^3\cos\tau\sin^2\tau,$$

$$\begin{aligned} T(\eta,\tau) \approx & -\hat{\xi}(\eta-1)\cos\tau + \hat{\xi}^2\sin^2\tau(\eta-1) - \tfrac{1}{2}\hat{\xi}^2(\eta^2-1)\cos^2\tau - 2\hat{\xi}\left(\int_\eta^1 \hat{v}_{,\tau}\,\mathrm{d}\eta\right)\cos\tau \\ & + \hat{\xi}\left[\int_\eta^1 (\hat{v}_{,\tau}+\hat{v}_0)\,\mathrm{d}\eta\right]\sin\tau + \hat{I}_m\hat{\xi}\frac{\partial^3\hat{v}}{\partial\eta^3}\bigg|_{\eta=1} + \hat{M}\hat{\xi}\cos\tau - \hat{M}\hat{\xi}^2\cos 2\tau \\ & - \tfrac{1}{2}\hat{M}\hat{\xi}^3\cos\tau\sin^2\tau + \tfrac{1}{2}\hat{M}\hat{\xi}^3\sin\tau\sin 2\tau, \end{aligned}$$

$$\alpha_{ij}^{cs} = \frac{1}{2}\left[\frac{(-1)^{i-j}-1}{(i-j)\pi} - \frac{(-1)^{i+j}-1}{(i+j)\pi}\right](1-\delta_{ij}), \quad \delta_{ij}: \text{ the Kronecker delta symbol},$$

$$\alpha_{ij}^{\eta ss} = \tfrac{1}{4}\delta_{ij} + \frac{1}{2}\left[\frac{(-1)^{i-j}-1}{(i-j)^2\pi^2} - \frac{(-1)^{i+j}-1}{(i+j)^2\pi^2}\right](1-\delta_{ij}),$$

$$a = \sigma_m,$$

$$b = \frac{\xi}{2\omega_m} f_{mm}^*,$$

$$c = \frac{\xi}{2\omega_m} f_{nm},$$

$$d = \frac{\xi}{2\omega_n} f_{mn},$$

$$e = \sigma_m + \sigma_{mn},$$

$$\Gamma_1 = 4(a^2 + b^2 + e^2) - 8(ab - cd + 2be),$$

$$\Gamma_2 = 16[(ae)^2 + (be)^2 + (cd)^2] + 32e[b(ae - cd) - acd],$$

$$\Gamma_1^* = 8a^2 - 8b^2 + 4e^2 + 8cd,$$

$$\Gamma_2^* = 32(ae)^2 - 32(be)^2 + 16(cd)^2 + 32cd(a^2 - b^2 + be - ae) + 16(a^2 - b^2)^2,$$

$$\Gamma_3^* = 64e^2(a^2 - b^2)^2 + 64(cd)^2(a - b)^2 - 128cde(a^3 - a^2b - ab^2 + b^3).$$

References

[1] M. Badlani, A. Midha, Member initial curvature effects on the elastic slider-crank mechanism response, *American Society of Mechanical Engineers, Journal of Mechanical Design* 104 (1982) 159–167.

[2] Z.G. Zhu, Y. Chen, The stability of the motion of a connecting rod, *American Society of Mechanical Engineers Journal of Mechanisms, Transmissions and Automation in Design* 105 (1983) 637–640.

[3] S.R. Hsieh, S.W. Shaw, Dynamic stability and nonlinear response of a flexible connecting rod: single-mode model, *Journal of Sound and Vibration* 170 (1994) 25–49.

[4] D. Halbig, D.G. Beale, Experimental observations of a flexible slider-crank mechanism at very high speed, *Nonlinear Dynamics* 7 (1995) 365–384.

[5] R.-F. Fung, Dynamic responses of the flexible connecting rod of a slider-crank mechanism with time-dependent boundary effect, *Computers and Structures* 63 (1997) 79–90.

[6] H. Hao, H.K. Cheong, S. Cui, Analysis of imperfect column buckling under intermediate velocity impact, *International Journal of Solids and Structures* 37 (2000) 5297–5313.

[7] S. Cui, H. Hao, H.K. Cheong, Dynamic bucking and post-buckling of imperfect columns under fluid-solid interaction, *International Journal of Solids and Structures* 38 (2001) 8879–8897.

[8] Y.M. Wang, The stability analysis of a slider-crank mechanism due to the existence of two-component parametric resonance, *International Journal of Solids and Structures* 36 (1999) 4225–4250.

[9] B.V. Viscomi, R.S. Ayre, Nonlinear dynamic response of elastic slider-crank mechanism, *American Society of Mechanical Engineers Journal of Engineering for Industry* 93 (1971) 251–267.

[10] A.H. Nayfeh, D.T. Mook, *Nonlinear Oscillations*, Wiley, New York, 1979.